The Kinase Domain Alters the Kinetic Properties of the Myosin IIIA Motor†

Andréa C. Dosé,‡ Shobana Ananthanarayanan,§ Judy E. Moore,§ Amoreena C. Corsa,‡ Beth Burnside,‡ and Christopher M. Yengo*,§

Department of Biology, University of North Carolina at Charlotte, Charlotte, North Carolina 28223, and Department of Molecular and Cell Biology, University of California, Berkeley, Berkeley, California 94720

Received October 26, 2007; Revised Manuscript Received December 17, 2007

ABSTRACT: Myosin IIIA is unique among myosin proteins in that it contains an N-terminal kinase domain capable of autophosphorylating sites on the motor domain. A construct of myosin IIIA lacking the kinase domain localizes more efficiently to the stereocilia tips and alters the morphology of the tips in inner ear hair cells. Therefore, we performed a kinetic analysis of myosin IIIA without the kinase domain (MIII ΔK) and compared these results with our reported analysis of myosin IIIA containing the kinase domain (MIII). The steady-state kinetic properties of MIII Δ*K* indicate that it has a 2-fold higher maximum actin-activated ATPase rate ($k_{cat} = 1.5 \pm 0.1$ s^{-1}) and a 5-fold tighter actin affinity ($K_{ATPase} = 6.0 \pm 1.4$ μM, and $K_{Actin} = 1.4 \pm 0.4$ μM) compared to MIII. The rate of ATP binding to the motor domain is enhanced in MIII Δ*K* ($K_1k_{+2} \approx 0.10 \pm 0.01$ μM^{-1}·s^{-1}) to a level similar to the rate of binding to MIII in the presence of actin. The rate of ATP hydrolysis in the absence of actin is slow and may be rate limiting. Actin-activated phosphate release is identical with and without the kinase domain. The transition between actomyosin.ADP states, which is rate limiting in MIII, is enhanced in MIII Δ*K*. MIII Δ*K* accumulates more efficiently at the tips of filopodia in HeLa cells. Our results suggest a model in which the activity and concentration of myosin IIIA localized to the tips of actin bundles mediates the morphology of the tips in sensory cells.

Myosin motor proteins generate force and motion through an ATP-dependent cyclic interaction with actin filaments (*1*). Mechanisms of regulation of myosin motor activity range from calcium-calmodulin to both heavy chain and light chain phosphorylation (*2*). Myosin III is unique in that it contains an N-terminal kinase domain that is capable of autophosphorylating sites on the motor domain (*3*, *4*). It is unclear what role autophosphorylation and the kinase domain play in regulating the function of myosin III in the cell.

Class III myosins were originally discovered in *Drosophila* eyes and designated as the NINAC protein (*5*−*7*). Two isoforms of myosin III, myosin IIIA and IIIB, have been identified in vertebrates (*8*, *9*). Expression of myosin IIIA has been found primarily in the retina and inner ear (*10*). Furthermore, disruption of the myosin IIIA gene leads to nonsyndromic deafness (*11*).

Cell biological studies suggest the kinase domain plays a role in regulation of myosin IIIA motor activity. Myosin IIIA localizes to the tips of actin bundles in the calycal processes of photoreceptors (*10*, *12*). In addition, studies in inner ear hair cells demonstrate myosin IIIA localizes to the tips of stereocilia, and a construct with the kinase domain removed localizes more efficiently to and seemed to alter the morphology of the stereocilia tips (*13*). Interestingly, cochlear expression of kinase deleted myosin IIIA resulted in expansion of a previously unidentified compartment found at the tips of stereocilia (*13*). These results suggest myosin IIIA may perform a critical mechanical function or mediate actin dynamics at the tips of actin bundles in sensory cells. Myosin IIIA was proposed to serve as a light-dependent transporter of arrestin and Gq alpha in invertebrate photoreceptors (*14*, *15*), but no transport function has been discovered in vertebrates. Thus, kinase-dependent regulation may be necessary to mediate actin-based transport or alter the morphology of the tips of actin bundles in sensory cells.

Recent results suggest that autophosphorylation of myosin IIIA reduces its affinity for actin and thus may be a mechanism for downregulating the motor (*16*). However, these studies were done with myosin IIIA lacking both the IQ domains and the kinase domain, and thus it is difficult to separate the effects of kinase removal from those due to lack of a lever arm. To understand how autophosphorylation regulates the motor domain and begin to explore the possibility of coupling between the motor and kinase domains, we have examined the kinetic properties of myosin IIIA containing the motor and two IQ domains but lacking the kinase domain. By comparing our results to our reported kinetic mechanism of the same myosin IIIA construct containing the kinase domain (*4*), we have determined the steps in the kinetic cycle altered by the presence of the kinase domain. These results allow us to propose a model that describes how the motor properties of myosin IIIA play a role in mediating the morphology of the stereocilia tips of inner ear hair cells.

† C.M.Y. is supported by grants from NIH(EY016419) and AHA-(Scientist Development Grant), and B.B. is supported by a grant from NIH(EY01750).

* To whom correspondence should be addressed. Christopher M. Yengo, Ph.D., Department of Biology, University of North Carolina at Charlotte, 9201 University City Blvd., Charlotte, North Carolina 28223. Phone: 704-687-8530. Fax: 704-687-3128. E-mail: cmyengo@uncc.edu.

§ University of North Carolina at Charlotte.

‡ University of California, Berkeley.

10.1021/bi7021574 CCC: $40.75
Published on Web 01/30/2008

EXPERIMENTAL PROCEDURES

Reagents. All reagents were the highest purity commercially available. ATP and ADP were prepared fresh from powder. *N*-Methylanthraniloyl(mant)-labeled 2′deoxy ADP and 2′deoxy ATP were prepared as described (*17*, *18*) or purchased from Jenna Biosciences. The mantATP[1] and mantADP concentrations were determined from absorbance measurements at 255 nm using ϵ_{255} of 23 300 $M^{-1}\cdot cm^{-1}$. ATP and ADP concentrations were determined by absorbance at 259 nm using ϵ_{259} of 15 400 $M^{-1}\cdot cm^{-1}$. Nucleotides were prepared prior to use in the presence of equimolar $MgCl_2$.

Myosin cDNA Construction and Protein Expression and Purification. We generated a construct of human myosin IIIA truncated after the second IQ domain (residues 1−1143) (MIII) and containing a C-terminal FLAG tag (DYKDDDDK) for purification purposes (*4*, *19*−*20*). A second construct was generated, identical to the first but with the kinase domain truncated (residues 324−1143) (MIII ΔK). Recombinant baculoviruses of myosin IIIA and calmodulin generated with the FastBac system (Invitrogen) were coexpressed in Sf9 cells. The myosin IIIA construct containing the kinase, motor, and 2IQ domains was previously demonstrated to be monomeric and contains no coiled-coil domain (*3*). We assumed the similar construct without the kinase domain is monomeric as well. The purity of MIII and MIII Δ*K* was assessed with Coomassie stained SDS gels. Myosin concentrations were determined using the Bio-Rad microplate assay using BSA as a standard (*4*). Actin was purified from rabbit skeletal muscle using an acetone powder method (*21*). Pyrene actin was generated by labeling actin with pyrene iodoacetamide (Molecular Probes) as described (*22*). All experiments were performed in KMg50 buffer (50 mM KCl, 1 mM EGTA, 1 mM $MgCl_2$, 1 mM DTT and 10 mM Imidazole-HCl, pH 7.0, 25 °C). The specific concentrations of ATP, ADP, MIII, and actin are indicated in the description of each experiment.

Kinase Activity. Autophosphorylation of MIII (0.5 μM) in the presence of 200 μM ATP was detected by western blot analysis using antiphosphothreonine and antiphosphoserine antibodies (Zymed Laboratories) as described (*4*). Densitometry analysis using NIH image software was used to determine the band intensities. The membranes were subsequently stripped and reprobed with an anti-FLAG antibody to detect total protein and verify even loading of samples.

Kinase activity was also determined by incubating MIII or MIII Δ*K* (2 μM) with [γ-^{32}P] ATP (200 μM ATP) for a 60 min period. The reaction was sampled at specific time points by removing an aliquot and quenching it with SDS-loading buffer. The samples were subjected to SDS PAGE and the degree of ^{32}P incorporation into the MIII heavy chain was visualized using a Typhoon phosphorimager.

Steady-State ATPase Activity. Steady-state ATP hydrolysis by MIII or MIII Δ*K* (50−100 nM) in the absence and presence of actin (0−70 μM) was examined using the NADH-linked assay (*4*, *23*) with a final MgATP concentration of 1 mM.

Actin-Cosedimentation Assay. MIII or MIII Δ*K* was equilibrated with actin (0−60 μM) and the ATP-regeneration system (2 mM phosphoenol pyruvate and 20 units/mL of pyruvate kinase); 2 mM ATP was added just prior to ultracentrifugation in a TLA 100.2 Beckman centrifuge rotor at 320 000× *g* for 20 min at 25 °C. The ADP concentration in the supernatant was determined by mixing a specified amount of the supernatant with the NADH mix and measuring the change in NADH absorbance as described in the *Steady-State ATPase Assays*. Equal amounts of the supernatant and pellet were subjected to SDS-PAGE and the fraction of MIII or MIII Δ*K* bound to actin was determined by quantifying the amount of MIII or MIII Δ*K* in the supernatant and pellet with densitometry using NIH image software. The actin-bound fraction was plotted as a function of actin concentration to determine the affinity of MIII or MIII Δ*K* for actin in the presence of ATP.

Acid Quench. To determine the equilibrium constant for ATP hydrolysis 1−2 μM MIII Δ*K* was mixed with 25 μM ATP containing [γ-^{32}P] ATP, allowed to react at 25 °C for 1−20 s, and quenched with quench solution (2N HCl, 0.35 M KH_2PO_4). The unhydrolyzed [γ-^{32}P]-ATP was removed using activated charcoal, and scintillation counting was used to determine ^{32}P concentrations (*4*, *24*, *25*). The number of moles of [γ-^{32}P]-ATP hydrolyzed per mole of myosin was used to calculate the phosphate burst and the equilibrium constant for ATP hydrolysis.

Stopped-Flow Measurements and Kinetic Modeling. Transient kinetic experiments were performed in an Applied Photophysics stopped-flow with a dead-time of 1.2 ms. A monochromator with a 2 nm band-pass was used for fluorescence excitation and cutoff filters were used to measure the emission. All optical filters were provided with the stopped-flow instrument. Light scatter was measured at 320 nm at 90°. Pyrene actin was excited at 365 nm, and the emission was measured using a 400 nm long pass filter. Mant labeled nucleotides were excited by energy transfer from tryptophans by exciting at 295 nm and the emission measured through a 400 nm long pass filter. Nonlinear least-squares fitting of the data was done with software provided with the instrument or KaleidaGraph (Synergy Software). Uncertainties reported are the standard error of the fits unless stated otherwise.

The kinetics of phosphate release were measured using phosphate-binding protein covalently labeled with *N*-[2-(1-maleimidyl)ethyl]-7-(diethylamino)coumarin-3-carboxamide-(MDCC−PBP) (generously provided by Howard White, Eastern Virginia University School of Medicine) (*26*). The fluorescence of MDCC−PBP, which increases several-fold in the presence of inorganic phosphate (*26*, *27*), was excited at 400 nm, and the emission was measured through a 425 nm long pass filter. Phosphate release was measured with a sequential mix experiment in which 2 μM myosin was mixed with 5 μM ATP and aged for 5 s to allow myosin to bind and hydrolyze the ATP, and then the M.ADP.Pi complex was mixed with actin (0−40 μM) (*4*) (final concentrations after mixing were 1.0 μM myosin, 2.5 μM ATP, 3 μM MDCC−PBP, and 0−40 μM actin). All solutions were preincubated with 7-methylguanosine (0.2 mM) and purine nucleoside phosphorylase (0.2 units·mL^{-1}) to remove background phosphate.

[1] Abbreviations: MIII, human myosin IIIA 2IQ; MIII Δ*K*, human myosin IIIA 2IQ (kinase removed); MDCC-PBP or PBP, *N*-[2-(1-maleimidyl) ethyl]-7-(diethylamino)coumarin-3-carboxamide-labeled phosphate binding protein; mantATP, *N*-methylanthraniloyl(mant)-labeled 2′deoxy ATP; mantADP, *N*-methylanthraniloyl(mant)-labeled 2′deoxy ADP.

Scheme 1

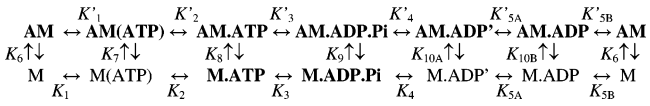

Kinetic modeling and simulations were performed with Pro-K software (Applied Photophysics) using the reaction scheme which has recently been used in kinetics studies of myosin IIIA, and other myosins (*4*, *28*−*30*) (see Scheme 1). In this scheme, myosin, actin, and actomyosin are represented by M, A, and AM, respectively. The rate and equilibrium constants are labeled on the basis of the reaction proceeding from left to right and those between the actin-associated and -dissociated steps proceeding in the dissociated direction. The main flux of the reaction pathway is shown in bold. The mixing ratio was one-to-one unless otherwise stated. All concentrations mentioned in the stopped-flow experiments are final concentrations unless stated otherwise.

HeLa Cell Culture and Transfections. HeLa cells were maintained and transfected as described (*31*) with the following changes. Initially, $1-2 \times 10^5$ cells were plated in 6-well plates and transfected with 1 μg DNA and 3 μL fugene reagent. After 24 h, the cells were trypsinized and replated onto polylysine coated coverslips in 6-well plates to promote filopodia formation. Fixation and imaging were done as previously described (*31*).

RESULTS

Protein Expression and Purification. The expression yields of human myosin IIIA 2IQ with or without the kinase domain coexpressed with calmodulin (MIII and MIII Δ*K*, respectively) in the baculovirus insect cell (Sf9) system were similar to previous studies (*4*). The purity of MIII and MIII Δ*K* following anti-FLAG affinity chromatography was approximately 95% based on Coomassie stained SDS-PAGE gels (expected molecular weights: MIII, 131 780 Da; and MIII Δ*K*, 93 469 Da) (Figure 1A). The stoichiometry of calmodulin to MIII or MIII Δ*K* in the final purified product was determined to be 2 calmodulins per myosin with densitometry analysis of SDS-PAGE gels (data not shown). All experiments were performed in KMg50 buffer and in the presence of 10-fold excess calmodulin to ensure that all the IQ domains of MIII or MIII Δ*K* had bound calmodulin. All steady-state and transient kinetic experiments were performed under identical conditions and with similar methods to directly compare the results to our kinetic characterization of MIII (*4*).

Kinase Activity. Western blot analysis was used to determine the phosphothreonine content of MIII Δ*K* and MIII purified from Sf9 cells (Figure 1B). A time course of autophosphorylation upon the addition of 200 μM ATP to 0.5 μM MIII was performed as previously described (*4*) and compared to MIII Δ*K*. In our previous work, we demonstrated two moles of phosphate were incorporated into MIII during a 60 min time course (*4*). There was no detectable phosphothreonine incorporated into MIII Δ*K* in the presence or absence of ATP (untreated). There was also very little phosphothreonine incorporation in MIII in the absence of ATP (untreated), whereas the enhancement of phosphothreonine content in the presence of ATP as a function of time

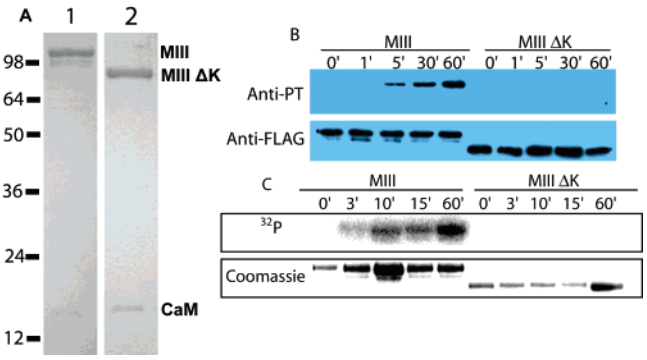

FIGURE 1: (A) SDS-PAGE of purified MIII and MIII Δ*K*. Lane 1 is the purified myosin III containing 2IQ domains (MIII) and lane 2 is purified myosin III with 2IQ domains but lacking the kinase domain (MIII Δ*K*). Calmodulin co-purified with the both MIII and MIII Δ*K*. The molecular weight markers (kDa) are labeled on the left. (B) Anti-phosphothreonine western blot. A time course of MIII autophosphorylation upon treatment with ATP demonstrates the increase in phosphothreonine content over a 60 min period (time points = 0, 1, 5, 30, and 60 min). MIII Δ*K* was also examined in the presence of ATP for the same time points as MIII. The blot was stripped and reprobed with anti-FLAG to demonstrate equal loading of samples. (C) Time course of MIII and MIII Δ*K* in the presence of [γ-^{32}P] ATP (200 μM) (time points = 0, 3, 10, 15, 60 min). Total protein was determined by Coomassie staining.

was similar to our previous study (*4*) (Figure 1B). Another time course was performed with anti-phosphoserine, which demonstrated that there was some phosphoserine content in MIII and none detectable in MIII Δ*K* in the absence of ATP (data not shown). The phosphoserine content in MIII increased as a function of time in the presence of ATP, albeit not as dramatically as phosphothreonine. In general, the anti-phosphoserine antibody was not as specific as the anti-phosphothreonine antibody, and therefore, a time course with MIII Δ*K* was not performed. Blots were stripped and reprobed with anti-FLAG to demonstrate that similar protein levels were present in each band. The kinase activity was also assayed by incubating MIII and MIII Δ*K* with [γ-^{32}P]-ATP (Figure 1C). The time course of MIII phosphorylation was similar to previous measurements (*4*) whereas no phosphorylation was detected with MIII Δ*K*. All kinetic experiments were performed with untreated MIII and MIII Δ*K*, which should mimic the dephosphorylated state (see discussion for further details).

Steady-State ATPase Activity. We examined the actin-activated ATPase activity of MIII Δ*K* using the NADH-coupled assay in KMg50 buffer at 25 °C, and compared it to our previously reported results with MIII (*4*) (Figure 2A). The rate of ATPase activity was plotted as a function of actin concentration and the data fit to the Michaelis Menten relationship. The maximum rate of ATPase activity (k_{cat}) of MIII Δ*K* was found to be 2-fold higher (1.5 ± 0.1 s^{-1}) than MIII (0.77 ± 0.08 s^{-1}), and the actin concentration at which one-half-maximal activity was achieved (K_{ATPase}) was found to be 5-fold lower (6.0 ± 1.4 μM) than MIII (34 ± 11 μM).

Actin Affinity in the Presence of ATP. Actin co-sedimentation assays were performed to determine the affinity of MIII Δ*K* for actin in the presence of ATP and ATP regeneration system. The ADP concentration after ultracentrifugation, determined by NADH absorbance, was found to be less than 10% of the total nucleotide concentration, which is higher than was reported for the NADH assay under equilibrium

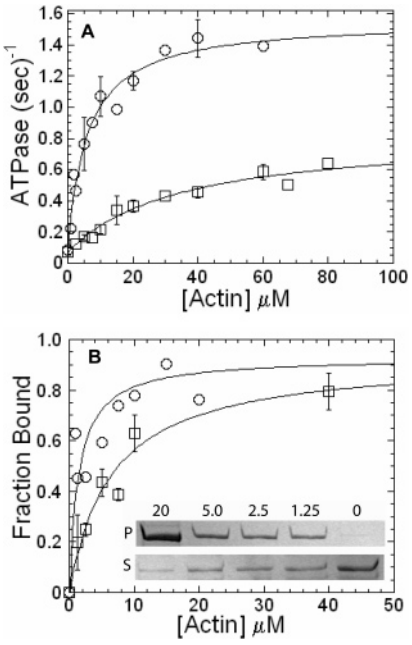

FIGURE 2: ATPase activity and actin binding affinity of MIII and MIII Δ*K*. (A) Steady-state ATPase rate of MIII (□, data from ref 4) and MIII Δ*K* (○) plotted as a function of actin concentration. The V_{MAX} and K_{ATPase} were determined by fitting the data to the Michaelis−Menten equation (see Table 1). (B) Affinity of MIII (data from ref 4) or MIII Δ*K* for F-actin was measured with the actin-cosedimentation assay in the presence of ATP (2 mM) and ATP-regeneration system. The plot of the fraction of MIII (□) and MIII Δ*K* (○) bound to actin as a function of actin concentration was fit to a hyperbola to determine the steady-state affinity for actin. The inset demonstrates the supernatant (S) and pellet (P) of MIII Δ*K* in the presence of 0, 1.25, 2.5, 5.0, and 20 μM actin. The data represent a summary of 3 separate experiments done with different protein preparations, and the error bars represent the standard deviation.

conditions (*23*). Figure 2B demonstrates that the steady-state affinity of MIII Δ*K* for actin is 5-fold tighter than MIII (K_{Actin} = 1.4 ± 0.4 and 7.0 ± 0.6 μM, respectively).

ATP-Binding. To examine the kinetics of ATP binding to MIII Δ*K* or acto-MIII Δ*K*, we used fluorescently labeled ATP (mantATP), which enhances fluorescence when bound to myosin (Figure 3). The rate of the mantATP fluorescence increase as a function of time was fit to a double exponential function at each mantATP concentration in the presence and absence of actin (1 μM MIII Δ*K* or acto-MIII ΔK). In the absence of actin, the slow phase of mantATP binding was 80−85% of the fluorescence signal, and this phase was linearly dependent on ATP concentration (K_1k_{+2} = 0.031 ± 0.005 $\mu M^{-1}\cdot s^{-1}$). The second, faster phase (~15 s^{-1}) was independent of mantATP concentration and was 15−20% of the signal. In the presence of actin, there were also two phases (0.8 fast and 0.2 slow) observed with the faster phase being linearly dependent on mantATP concentration ($K'_1k'_{+2}$ = 0.116 ± 0.013 $\mu M^{-1}\cdot s^{-1}$) and the slower phase (0.15−0.25 s^{-1}) being independent of mantATP concentration. The y-intercept of the linear fits was higher in the presence compared to the absence of actin (1.5 ± 0.1 s^{-1} and 0.35 ± 0.05 s^{-1}).

To determine the kinetics of unlabeled ATP binding to myosin and actomyosin III Δ*K*, we examined ATP binding by kinetic competition with mantATP (Figure 3B) (*4*, *25*). MIII Δ*K* or actomyosin III Δ*K* (0.5 μM) was mixed with 5

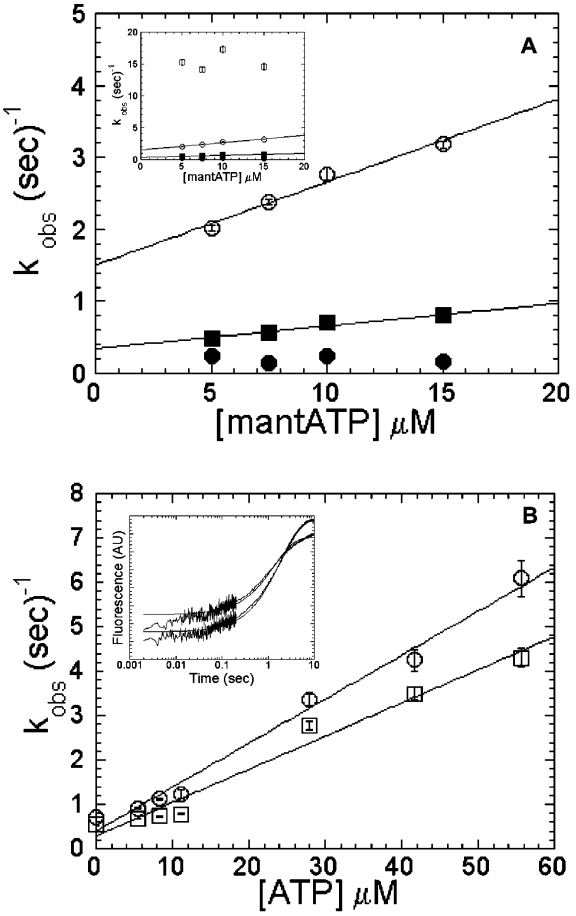

FIGURE 3: ATP binding to MIII Δ*K* and acto-MIII Δ*K*. (A) Rate of mantATP binding to MIII Δ*K* and acto-MIII Δ*K* monitored with mantATP fluorescence. The fluorescence transients were fit to a two exponential function at all mantATP concentrations in the presence [relative amplitudes: fast = 0.80 (○), slow = 0.20 (●)] and absence [amplitudes: fast = 0.14 (□, inset), slow = 0.86 (■)] of actin. (Inset) Fast phase of the fluorescence transient in the absence of actin (□). (B) Rate of ATP binding was also measured by kinetic competition with mantATP (MIII Δ*K*, □; acto-MIII Δ*K*, ○). (Inset) Fluorescence transients observed with two different mantATP/ATP concentrations in the absence of actin (a, 5 μM mantATP and 0 μM ATP with k_{obs} = 0.54 ± 0.01 s^{-1}, b, 5 μM mantATP and 5 μM ATP with k_{obs} = 0.68 ± 0.01 s^{-1}).

μM mantATP and varying concentrations of ATP. The mantATP fluorescence transients were dominated by the slow phase in the absence of actin and fast phase in the presence of actin (≥90% of the signal) and were linearly dependent on ATP concentration. In the absence of actin, a second-order binding constant of 0.075 ± 0.005 $\mu M^{-1}\cdot s^{-1}$ was found. In the presence of actin, we obtained a second-order binding constant of 0.099 ± 0.005 $\mu M^{-1}\cdot s^{-1}$. The rate of binding in the presence of actin was similar to the second-order binding constant for ATP binding determined by pyrene actin and light scatter (Figure 4). The amplitude of the mantATP fluorescence decreased as a function of ATP concentration. This allowed us to determine the apparent affinity of MIII Δ*K* and acto-MIII Δ*K* for ATP using a standard competitive binding equation ($K_d \approx 8$ μM for both MIII Δ*K* and acto-MIII Δ*K*) (data not shown).

We measured the rate of ATP-induced formation of weakly bound actomyosin III Δ*K* using pyrene actin (Table 2). Strongly bound myosin quenches pyrene actin whereas upon ATP binding the fluorescence recovers due to population of

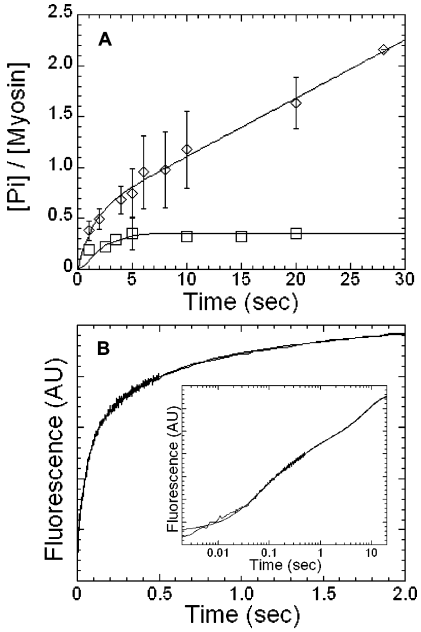

FIGURE 4: Equilibrium constant for ATP hydrolysis determined by acid quench and phosphate release experiments. (A) Myosin III ΔK (1.0−2.0 μM) was mixed with [γ-^{32}P]-ATP (25 μM) and manually quenched at specific time points. The data represent the average of three experiments (◊) done with three separate protein preparations, and the error bars represent the standard deviation of the mean. The data was fit to a single-exponential burst, modeled to be the Pi-burst, followed by a steady-state rate (burst rate = 0.71 ± 0.22 s^{-1}, amplitude was 0.53 ± 0.05 μM Pi per μM MIII ΔK, steady-state rate = 0.06 ± 0.01 s^{-1}). The rate and equilibrium constant for ATP hydrolysis were also determined by examining the amount of MIII ΔK that was capable of actin-activated phosphate release after a sequential mix with different age times (□) (final reaction conditions: 1 μM MIII ΔK, 2.5 μM ATP, 20 μM actin, 3 μM PBP). The phosphate release amplitude was plotted as a function of age time and fit to a kinetic simulation to estimate the rate and equilibrium constants for ATP hydrolysis (k_{+3} = 1.8 s^{-1}, k_{-3} = 1.2 s^{-1}, K_3 = 1.5). (B) Phosphate release transient after a 20 s age time was best fit to a three exponential function (k_{obs} = 19.3 ± 0.4, 2.8 ± 0.1, and 0.14 ± 0.01 s^{-1}, relative amplitudes = 0.33, 0.27, and 0.4, respectively). (Inset) The phosphate release transient on a log time scale.

the weakly bound states of myosin. The linear fit of the ATP binding rates as a function of ATP concentration (in the concentration range of 0−500 μM ATP) was used to determine the second-order rate constant for ATP binding ($K'_1k'_{+2}$). This rate constant determined for MIII ΔK ($K'_1k'_{+2}$ = 0.065 ± 0.007 $\mu M^{-1}\cdot s^{-1}$) was found to be similar to that measured with mantATP (Table 2). The hyperbolic fit of the data allowed us to determine the equilibrium constant ($1/K'_1$ = 4056 ± 853 μM), as well as the maximum rate of ATP binding (k'_{+2} = 265 ± 29 s^{-1}) to pyrene actomyosin III ΔK.

Similar experiments were performed by using the light scatter signal to monitor ATP-induced dissociation of actomyosin III ΔK (Table 2). The second-order rate constant for ATP binding to actomyosin III ΔK was found to be similar to that measured with pyrene actin ($K'_1k'_{+2}$ = 0.054 ± 0.005 $\mu M^{-1}\cdot s^{-1}$), as was the equilibrium constant for ATP binding to actomyosin III ΔK ($1/K'_1$ = 4591 ± 1063 μM) and the maximum rate of ATP-induced dissociation (k'_{+2} = 248 ± 34 s^{-1}). The amplitudes of the light scatter transients were plotted as a function of ATP concentration, which allowed us to determine the apparent affinity of actomyosin III ΔK

Table 1: Steady-State Parameters of the MIII Motor ATPase Cycle

steady-state parameters	MIII	MIII (ΔK)
V_0 $(sec)^{-1a}$	0.07 ± 0.03	0.08 ± 0.02
k_{cat} $(sec)^{-1b}$	0.77 ± 0.08	1.5 ± 0.1
K_{ATPase} (μM)[c]	34 ± 11	6.0 ± 1.4
K_{Actin} (μM)[d]	7.0 ± 0.6	1.4 ± 0.4

[a] Steady-state ATPase activity in the absence of actin measured with the NADH coupled assay. [b] Maximum rate of actin-activated ATPase measured with the NADH coupled assay. The values for K_{ATPase} and k_{cat} were determined from the fit of the data in Figure 2 to the equation: $[V_0 + (k_{cat}\,[Actin])/(K_{ATPase} + Actin)]$. [c] Actin concentration at which the actin-activated ATPase rate is one-half-maximal from the NADH assay. [d] Dissociation constant of MIII and MIII ΔK for F-actin in the presence of ATP and ATP-regeneration system, measured by actin cosedimentation.

for ATP (K_d = 22 ± 11 μM) (data not shown). The apparent affinity can be modeled with the equation $K_d = k'_{-2}/K'_1k'_{+2}$, which assumes the initial interaction is a rapid equilibrium (K'_1) that is followed by an isomerization step (K'_2). These results suggest that the rate of the isomerization from the weakly bound to the strongly bound conformation (K'_2) limits the overall rate of ATP-induced dissociation of myosin III ΔK from actin. Based on the ATP binding rates that pass relatively close to the origin and the slow rate of the reverse isomerization step estimated from the above equation ($k'_{-2} \approx 1\ s^{-1}$), we conclude that ATP binding to the motor domain is highly favorable.

ATP Hydrolysis. The equilibrium constant for ATP hydrolysis was determined by acid quench experiments with [γ-^{32}P]ATP (see *Experimental Procedures*) (Figure 4). After mixing 25 μM [γ-^{32}P]ATP with 1.0−2.0 μM MIII ΔK the reaction was quenched at time points from 1 to 20 s. The amount of ATP hydrolyzed per myosin was plotted as a function of time in Figure 4 (average of 3 separate MIII ΔK preparations). The data fit well to a single-exponential burst (0.71 ± 0.22 s^{-1}) followed by a steady-state rate (0.06 ± 0.01 s^{-1}). The amplitude of the Pi-burst was found to be 0.53 ± 0.05 mol Pi/mol myosin. The data were corrected for the amount of MIII ΔK that did not bind ATP, using the affinity determined in the ATP binding experiments (K_d = 8 μM). The amplitude of the burst was used to estimate the equilibrium constant for ATP hydrolysis (K_3 = 1.2) using the following equation: Burst = $K_3/(1+K_3)$.

We also examined the rate of ATP hydrolysis by performing a sequential mix experiment in which MIII ΔK (2 μM) was first mixed with ATP (5 μM), allowed to age for various time periods (1−20 s), and then mixed with actin and phosphate-binding protein (final reaction conditions: 1 μM MIII ΔK, 2.5 μM ATP, and 20 μM actin, and 3 μM phosphate-binding protein) (Figure 4). The amplitude of rapid phosphate release is indicative of the concentration of MIII ΔK in the M.ADP.Pi state. A standard curve with inorganic phosphate was used to convert the fluorescence amplitude into moles of phosphate released. The amplitude of rapid actin-activated phosphate release was dependent on the age time and was fit to a kinetic simulation using the previously measured ATP binding rate constants (K_1k_{+2} = 0.37 s^{-1}, k_{-2} = 0.6 s^{-1}). The kinetic simulation allowed us to estimate the rate and equilibrium constants for ATP hydrolysis (k_{+3} = 1.8 s^{-1}, k_{-3} = 1.2 s^{-1}, K_3 = 1.5). The amplitude was corrected for the MIII ΔK that did not bind actin ($1/K_9$ = 29 μM, see phosphate release experiments, Figure 6). The

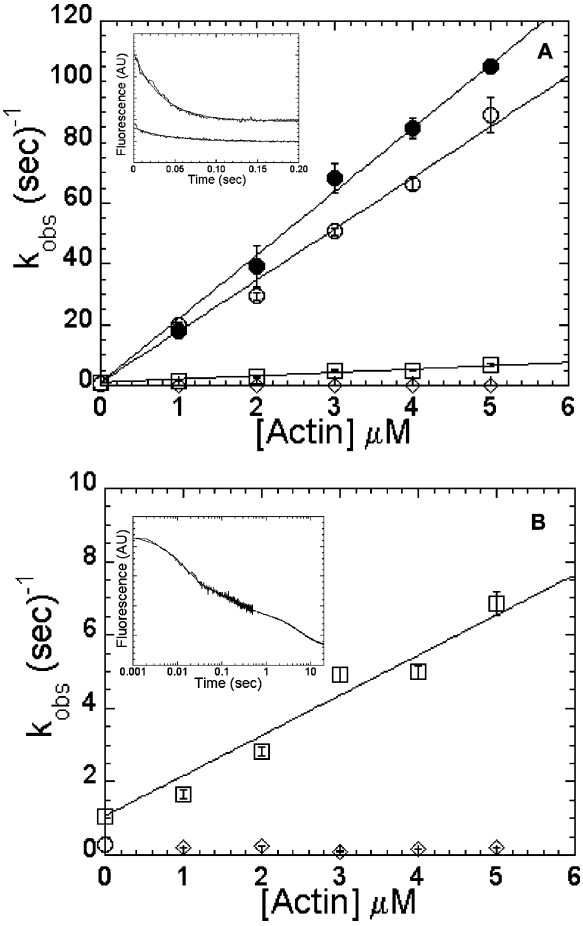

FIGURE 5: Binding of MIII Δ*K* to pyrene actin filaments. (A) Pyrene actin fluorescence transients upon mixing MIII Δ*K* with 5- to 10-fold excess pyrene actin were fit to a single-exponential function at each pyrene actin concentration in the absence of nucleotide and a three exponential function in the presence of ADP (0.5 mM). The rate of pyrene actin fluorescence quenching in the absence of nucleotide (●) and the fast phase in the presence of ADP (○), were linearly dependent on pyrene actin concentration. (Inset) Fast phase of the fluorescence transients in the absence, upper trace, and presence of ADP, lower trace. (B) In the presence of ADP, the intermediate phase (□) of binding to pyrene actin was linearly dependent on actin concentration, while the slow phase (◇) was independent of actin concentration. (Inset) Fluorescence transient shown on a log time scale from 0.5 μM MIII Δ*K* binding to 4 μM pyrene actin and the fit to a three exponential function (k_{obs} = 66 ± 2, 5.0 ± 0.2, and 0.17 ± 0.01 s^{-1}, amplitudes = 0.45. 0.23, 0.32, respectively).

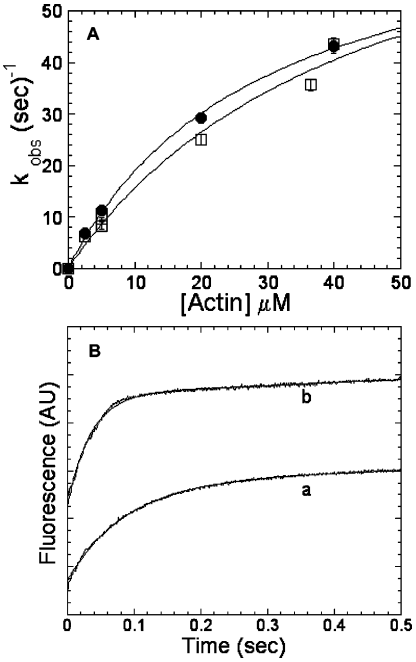

FIGURE 6: Actin-activated phosphate release from MIII and MIII Δ*K*. (A) Rate of the phosphate burst in MIII Δ*K* was hyperbolically dependent on actin concentration (●). The phosphate release data previously reported for MIII (*4*) is shown for comparison (□). (B) Fluorescence transients of phosphate release from MIII Δ*K* in the presence of actin which contain a burst phase followed by two slower phases. The burst was fit to a single-exponential function followed by a linear phase to determine the rate of phosphate release at each actin concentration. Final reaction conditions: 1 μM MIII, 2.5 μM ATP, 3 μM phosphate binding protein, 5 μM actin [transient a, k_{obs}(burst) = 13.2 ± 0.1 s^{-1}), and 20 μM actin (transient b, k_{obs}(burst) = 29.2 ± 0.3 s^{-1}].

phosphate release transients with a 10, 15, and 20 s age time were best fit by a three exponential function (k_{obs} for 20 s age time = 19.3 ± 0.4 s^{-1}, 2.8 ± 0.1 s^{-1}, and 0.14 ± 0.01 s^{-1}; relative amplitudes = 0.33, 0.27, 0.40, respectively) (Figure 4B). The three phases are consistent with rapid actin-activated phosphate release (fast), ATP hydrolysis (intermediate), and ATP binding and/or phosphate release in the absence of actin (slow), respectively. The relative amplitudes of the phosphate release and ATP hydrolysis rates are consistent with the equilibrium constant for hydrolysis measured in the ^{32}P experiments.

Binding to Pyrene Actin Filaments. We examined the binding of MIII Δ*K* to pyrene actin filaments (5−10 fold excess over MIII Δ*K*) by examining the rates of association and dissociation in the presence of ADP (0.5 mM) and absence of nucleotide (Figure 5). The association rates in the absence of nucleotide were fit to a single-exponential function and found to be linearly dependent on actin concentration. The association rates in the presence of ADP were fit to a three exponential function with the fast and intermediate phases dependent on actin concentration, while the slow phase was independent of actin concentration (k_{obs} ≈ 0.2 s^{-1}) (relative amplitudes: slow = 0.34, intermediate = 0.24, fast = 0.42). The rate of the fast phase of MIII Δ*K* binding to actin was similar in the presence of ADP (k_{+10} = 16.8 ± 0.4 μM^{-1}·s^{-1}) and in the absence of nucleotide (k_{+6} = 21.2 ± 0.4 μM^{-1}·s^{-1}). The intermediate phase in the presence of ADP was found to have an association rate of 1.1 ± 0.4 μM^{-1}·s^{-1} (Figure 5B). The rate of dissociation from actin was also monitored by mixing pyrene actomyosin III Δ*K* with excess unlabeled actin filaments. The dissociation rates were fit to a two exponential function in the absence of ADP (k_{-6} = 2.1 ± 0.13 and 0.40 ± 0.02 s^{-1}) and presence of ADP (k_{-10} = 1.1 ± 0.1 and 0.30 ± 0.01 s^{-1}) (relative amplitudes for slow and fast phases were similar in the presence and absence of ADP: 0.35 and 0.65, respectively). The y-intercepts of the fast and intermediate phases of MIII Δ*K* binding to actin in the presence of ADP were very similar to the fast and slow dissociation rates. Thus, the data was modeled with two different ADP states, one with a weak actin affinity ($1/K_{10A}$ = 1.1 ± 0.1 μM) and another with a strong actin affinity ($1/K_{10B}$ = 0.020 ± 0.001 μM). The data in the absence of nucleotide also suggest the presence of weak ($1/K_{6(weak)}$ = 0.10 ± 0.01 μM) and strong ($1/K_{6(strong)}$ = 0.020 ± 0.001 μM) actin binding rigor states,

having similar association rates but different dissociation rates.

Phosphate Release. We examined the rate of actin-activated phosphate release using the sequential mix experiment described in *Experimental Procedures* (Figure 6). The rate of phosphate release in the presence and absence of actin was determined by mixing 2 μM MIII ΔK with 5.0 μM ATP, allowing the reaction to age for 5 s and then mixing with phosphate binding protein and various concentrations of actin (0−40 μM). A standard curve with inorganic phosphate allowed us to determine the concentration of phosphate release during the reaction. In the absence of actin, there was no phosphate burst observed and a linear fit of the transient was found to be similar to the steady-state ATPase rate expected at this ATP concentration (0.02 mol Pi·mol myosin^{-1}·s^{-1}) (data not shown). In the presence of actin, a burst was observed (Figure 6) followed by a slower linear phase ($\sim$0.1 s^{-1}). The burst rate was plotted as a function of actin concentration and fit to a hyperbolic relationship, to determine the maximum rate of phosphate release (k'_{+4} = 74 ± 5 s^{-1}) and affinity for actin in the ADP.Pi state ($1/K_9$ = 29 ± 4 μM) (Figure 6). The results are very similar to phosphate release in MIII in that phosphate release is rapid and the affinity for actin in the ADP.Pi state is weak (k'_{+4} ≥ 74 ± 5 s^{-1} and $1/K_9$ ≥ 29 ± 4 μM). The amplitude of the burst phase corresponded to a phosphate burst of 0.16 μM Pi at 40 μM actin, which was in good agreement with our expectations based on the predicted amount of MIII ΔK in the M.ADP.Pi state and the affinity for actin in the M.ADP.Pi state (see also Figure 4).

ADP Binding to and Dissociation from Myosin III ΔK and Actomyosin III ΔK. The rate of ADP binding to myosin III ΔK (0.5 μM) and actomyosin III ΔK (0.5 μM MIII ΔK: 5.0 μM actin) was monitored with mantADP (Table 2). There was a biphasic transient observed upon mantADP binding to myosin or actomyosin III ΔK. The transients were similar to those observed in MIII except they lacked the rapid phase which we had previously assigned to mantADP binding to the kinase domain. In the presence and absence of actin the fast phase was dependent on mantADP concentration. The data was modeled as a two step binding to MIII ΔK, in which the mantADP fluorescence was sensitive to both states. In the absence of actin, the linear dependence of the fast phase on mantADP concentration allowed us to determine the second-order binding constants in the absence (k_{-5B} = 0.51 ± 0.12 μM^{-1}·s^{-1}) and presence of actin (k'_{-5B} = 0.29 ± 0.07 μM^{-1}·s^{-1}). The slow phase in the absence and presence of actin was independent of mantADP concentration in the concentration range measured (0.3−0.4 and 0.5−1.2 s^{-1}, respectively). The amplitudes of each of the fast and slow phases were similar at each mantADP concentration in the absence (relative amplitudes = 0.70 and 0.30, respectively) and presence (relative amplitudes = 0.78 and 0.22, respectively) of actin.

The rate of mantADP release from myosin III ΔK and actomyosin III ΔK was determined by mixing actomyosin III ΔK (0.5 μM MIII ΔK: 2.5 μM actin) or MIII ΔK (0.5 μM) in the presence of 12.5 μM mantADP with 5 mM ATP (Table 2). The rate of mantADP release from MIII ΔK and actomyosin III ΔK was also biphasic. The fast phases in the absence (5.3 ± 0.5 s^{-1}) and presence (8.8 ± 0.4 s^{-1}) of actin were slightly lower than the y-intercept determined from the direct binding experiments described above. The slow phase was found to be similar in the absence (0.45 ± 0.09 s^{-1}) and presence (0.62 ± 0.07 s^{-1}) of actin. The relative amplitudes of the fast and slow phases were slightly different in the absence (0.66 and 0.34, respectively) and presence of actin (0.73 and 0.27, respectively). The fast and slow mantADP release rates in the presence of actin are in reasonably good agreement with the release of unlabeled ADP from actomyosin III measured with light scatter or pyrene actin (Figure 7B).

We analyzed the two-step mantADP binding to the motor domain of myosin III ΔK and actomyosin III ΔK with equations outlined in Henn and De La Cruz (*28*). This model was also used in our kinetic analysis of MIII (*4*). The

Table 2: Summary of Rate and Equilibrium Constants in the Myosin IIIA Motor ATPase Cycle

rate/equilibrium constant	MIII	MIII ΔK
ATP binding and hydrolysis		
K_1k_{+2} (μM$^{-1}\times$sec^{-1})[a]	0.010 ± 0.004	0.031 ± 0.005
K_1k_{+2} (μM$^{-1}\times$sec^{-1})[b]	0.002 ± 0.001	0.075 ± 0.005
K_3[c]	9	1.5
$K'_1k'_{+2}$(μM$^{-1}\times$sec^{-1})[a]	0.005 ± 0.002	0.116 ± 0.013
$K'_1k'_{+2}$ (μM$^{-1}\times$sec^{-1})[b]	0.043 ± 0.010	0.099 ± 0.005
$K'_1k'_{+2}$ (μM$^{-1}\times$sec^{-1})[d]	0.022 ± 0.001	0.054 ± 0.005
$1/K'_1$ (μM)[d]	11 144 ± 2319	4591 ± 1063
k'_{+2}(sec^{-1})[d]	246 ± 38	248 ± 34
ADP binding		
k'_{+5B} (sec^{-1})[e]	6.8 ± 0.2	6.5 ± 0.1
k'_{-5B}(μM$^{-1}\times$sec^{-1})[e]	1.0 ± 0.1	0.4 ± 0.1
K'_{5B} (μM)[e]	6.8 ± 0.4	16.4 ± 2.2
*k'_{+5A} (sec^{-1})[e,f]	0.60 ± 0.10	0.67 ± 0.20
*k'_{+5A} (sec^{-1})[f,g]	0.97 ± 0.03	0.62 ± 0.07
*k'$_{-5A}$ (sec^{-1})[f,g]	0.54 ± 0.08	0.50 ± 0.10
*K'_{5A}[f,g]	1.8 ± 0.3	1.2 ± 0.3
k'_{+5B} (sec^{-1})[g]	9.84 ± 0.25	8.5 ± 0.4
k'_{-5B} (μM$^{-1}\times$sec^{-1})[g]	0.29 ± 0.11	0.29 ± 0.07
K'_{5B} (μM)[g]	34 ± 14	29.1 ± 7.3
k_{+5A} (sec^{-1})[g]	1.00 ± 0.24	0.45 ± 0.09
k_{-5A} (sec^{-1})[g]	0.88 ± 0.11	0.35 ± 0.10
K_{5A}[g]	1.1 ± 0.3	1.2 ± 0.4
k_{+5B} (sec^{-1})[g]	9.26 ± 1.55	4.8 ± 1.3
k_{-5B} (μM$^{-1}\times$sec^{-1})[g]	0.31 ± 0.09	0.51 ± 0.12
K_{5B} (μM)[g]	30 ± 11	9.4 ± 3.4
Pi release		
k'_{+4} (sec^{-1})[h]	85 ± 17	74 ± 5
$1/K_9$[h]	44 ± 15	29 ± 4
Actin binding		
k_{+6} (μM$^{-1}\times$sec^{-1})[i]	11.4 ± 0.4	21.2 ± 0.4
k^{-6} (sec^{-1})[i]	1.5 ± 0.1	0.40 ± 0.02
$1/K_6$ (μM)[i]	0.13 ± 0.01	0.020 ± 0.001
k_{+10A} (μM$^{-1}\times$sec^{-1})[i]	14.6 ± 0.6	16.8 ± 0.4
k_{-10A} (sec^{-1})[i]	1.2 ± 0.1	0.30 ± 0.01
$1/K_{10B}$ (μM)[i]	0.08 ± 0.01	0.020 ± 0.001
k_{+10A} (μM$^{-1}\times$sec^{-1})[i]	NA	1.1 ± 0.1
k_{-10A} (sec^{-1})[i]	NA	1.1 ± 0.1
$1/K_{10A}$ (μM)[i]	NA	1.0 ± 0.1
$1/K_{10A}$ (μM)[j]	5.0	NA

[a] mantATP fluorescence. [b] ATP binding by competition with mantATP. [c] Acid quench with [γ-^{32}P]ATP. [d] ATP-induced dissociation monitored by light scatter. [e] ADP release by competition with ATP-induced dissociation monitored by light scatter or pyrene actin. [f] Note the rate and equilibrium constants defining K'_{5A} were modeled with an off-pathway intermediate ($K_{10\alpha}$, see Discussion) in MIII ΔK. [g] mantADP fluorescence. [h] Phosphate binding protein. [i] Pyrene actin fluorescence. [j] Predicted from kinetic simulation of steady-state actin binding data (not determined by simulation with MIII ΔK because this state is not a significantly populated steady-state intermediate in the MIII ΔK ATPase cycle).

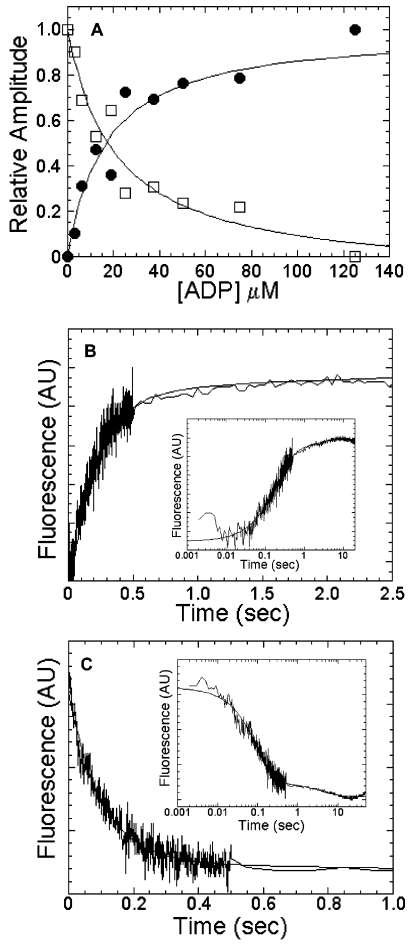

FIGURE 7: ADP binding to and dissociation from acto-MIII Δ*K*. (A) Pyrene acto-MIII Δ*K* (0.5 μM) in the presence of varying concentrations of ADP was mixed with 5 mM ATP. The amplitude of the slow phase (●) increased as a function of ADP concentration, while the amplitude of the fast phase (□) decreased. The ADP concentration dependence of the amplitude of the slow phase was fit to a hyperbola to determine the dissociation constant for ADP binding to MIII Δ*K* ($K_{5B}' = 16.4 \pm 2.2$ μM). B) The rate of ADP-release measured with pyrene actomyosin III Δ*K* as described for panel A except at a higher pyrene actin concentration (final conditions: 0.5 μM MIII Δ*K*, 5 μM pyrene actin, 100 μM ADP, 5 mM ATP). The fluorescence transients were best fit by a two exponential function containing fast (5.0 ± 0.2 s^{-1}) and slow (0.67 ± 0.20 s^{-1}) components (relative amplitudes, fast = 0.9, slow = 0.1). (Inset) Same fluorescence transient on a log time scale. (C) The rate of mantADP release following binding to actin in the M.ADP.Pi state. MIII Δ*K* (2.25 μM) was mixed with 12.5 μM mantATP, aged for 4 s and then mixed with 20 μM actin and 0.5 mM ADP (final reaction conditions: 1.13 μM MIII Δ*K*, 6.25 μM mantATP, 20 μM actin, and 0.5 mM ADP). The mant fluorescence decay was fit to a two exponential function ($k_{obs} = 9.9 \pm 0.2$ and 0.25 ± 0.02 s^{-1}). (Inset) Same transient on a log time scale.

calculated dissociation constant for the overall affinity for mantADP was 3-fold weaker in the presence compared to the absence of actin (K_d (overall) = 16 ± 7 μM and 5 ± 3 μM, respectively). The ratio of amplitudes of the slow and fast phases for mantADP dissociation are in reasonable agreement with the determined equilibrium constant (K_{5A}) for the transition between the two proposed ADP states in the presence and absence of actin [$K'_{5A} = 1.2$, dissociation amplitude ratio (fast phase/slow phase) ≈ 2.8; $K_{5A} = 1.2$, dissociation amplitude ratio (fast phase/slow phase) ≈ 1.9]. However, the amplitudes from the mantADP association experiments are slightly different than what is expected from the two-state model in the presence and absence of actin (fast/slow association amplitude ratio ~3.5 and ~2.3, respectively).

We also examined the rate of ADP release from pyrene actomyosin III Δ*K* by performing ATP-induced dissociation (5000 μM ATP) experiments with 0.5 μM actomyosin III Δ*K* in the presence of varying concentrations of ADP (Figure 7A). The fluorescence transients contained two phases at all ADP concentrations measured (~120 and ~6.5 s^{-1}). The slow phase was modeled to be ADP release and the fast phase modeled to be ATP-induced dissociation. The amplitudes of the slow phase increased while the fast phase decreased as a function of ADP concentration. The amplitudes were fit to a hyperbolic function to determine the apparent affinity of actomyosin III Δ*K* for ADP ($1/K'_{5B} = 16.4 \pm 2.2$).

We also measured ADP release from actomyosin III Δ*K*, as described above but in the presence of a higher actin concentration (final conditions: 5.0 μM pyrene actin, 0.5 μM MIII Δ*K*, 100 μM ADP, and 5 mM ATP) as was performed for MIII (*4*) (Figure 7B). We observed a fast and a slow phase of ADP-release with the fast phase dominating the signal (amplitude was 90% of the total). The fast and slow phases ($k'_{5B} = 5.0 \pm 0.2$; $k'_{5A} = 0.67 \pm 0.20$) were similar to those measured with mantADP, while the relative amplitudes were different. The mant probe may alter the equilibrium between actomyosin.ADP states as was found in a myosin VII study (*28*).

Actin-Activated ADP-Release. We performed a sequential mix experiment in which MIII Δ*K* (2.25 μM) was mixed with 12.5 μM mantATP, aged for 4 s to allow MIII Δ*K* to populate the M.ADP.Pi state, and then mixed with 20 μM actin in the presence of 500 μM ADP (Figure 7C) (final reaction conditions: 1.13 μM MIII Δ*K*, 6.25 μM mantATP, 20 μM actin, and 0.5 mM ADP). The mant fluorescence followed a two exponential function with rate constants of 9.9 ± 0.2 and 0.25 ± 0.03 s^{-1} (relative amplitudes, 0.85 and 0.15, respectively). We obtained similar results when the age time was increased to 20 s (data not shown). The transients were dominated by the fast rate, which is similar to the fast phase of mantADP release measured in the mantADP binding and release experiments (Table 2). Similar experiments were performed in the absence of actin and the rate of the mant fluorescence transient after a 20 s age time was found to be 0.18 ± 0.01 s^{-1} (data not shown). This rate is similar to the slow phase measured in the presence of actin (Figure 7C), which likely represents the rate of phosphate release in the absence of actin (see also Figure 4B).

HeLa Cell Localization. To examine the effect that the loss of the kinase domain would have on heterologously expressed myosin IIIA we transfected HeLa cells with full length myosin IIIA containing an N-terminal GFP tag with and without the kinase domain (GFP.MIII Full and GFP.MIII Full ΔK) (Figure 8). Here we used constructs that included the tail domain since a functional 3THDII (Myosin III Tail Homology Domain II) is necessary for tip localization in HeLa cells (*31*). Cell counting yielded that 86% of the cells transfected with the full-length myosin IIIA Δ*K* construct ($n = 200$) exhibited a concentration of fluorescence at the tips of filopodia, whereas only 41% of cells transfected with GFP.MIII Full ($n = 200$) exhibited a concentration of

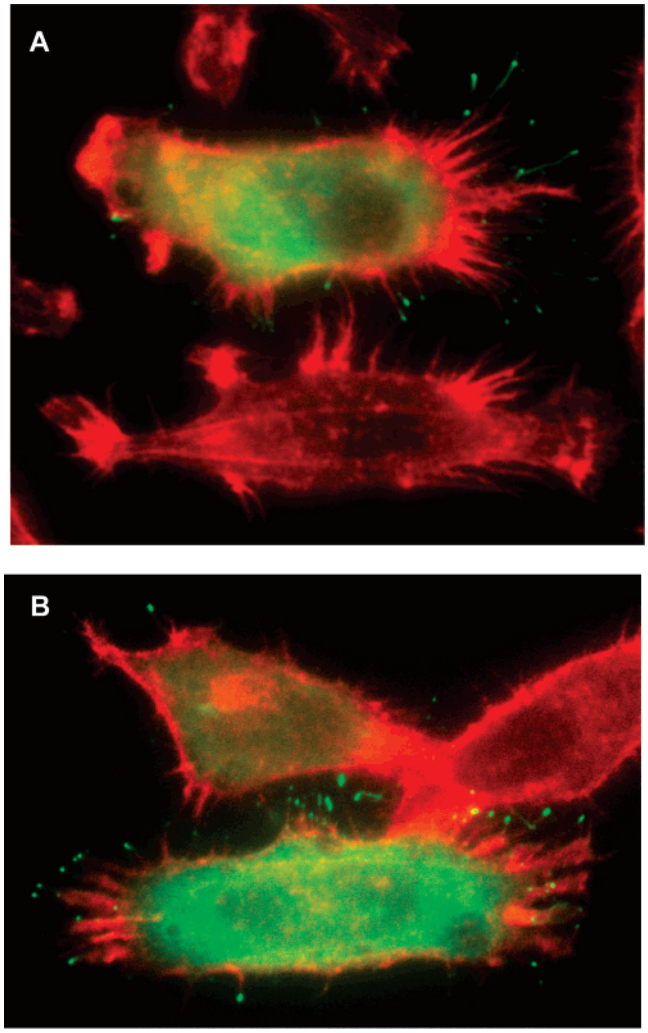

FIGURE 8: HeLa cells were transfected with plasmids encoding a full length wild type myosin IIIA tagged with GFP (GFP.MIII Full) (A) or full length myosin IIIA with the kinase domain removed (GFP.MIII Full Δ*K*) (B), and analyzed by fluorescence microscopy. The amount of GFP.MIII Full and GFP.MIII.Full Δ*K* protein localized along the filopodia and at the filopodial tips was compared. The F-actin cytoskeleton was visualized with Texas Red-X phalloidin.

fluorescence at the tips of filopodia. These results suggest that the mechanism responsible for tip localization, whether it be ability/likelihood of myosin IIIA to reach the tips or lack of its ability to leave (or be recycled from) the tips, is enhanced when the kinase domain is not present in the molecule.

DISCUSSION

*Overall Comparison of Myosin III and Myosin III Δ*K* Kinetics.* We have examined the key rate and equilibrium constants in the motor ATPase cycle of myosin IIIA lacking the kinase domain but containing the first two IQ motifs. The current results were compared to the motor ATPase mechanism of myosin IIIA containing the kinase domain (*4*), directly demonstrating the impact of the kinase domain on the kinetic properties of the myosin IIIA motor. The steady-state results demonstrate MIII Δ*K* has a 2-fold higher k_{cat} and 5-fold higher steady-state actin affinity. The k_{cat} is enhanced in the MIII Δ*K* because of a faster transition between actomyosin.ADP-states. Thus, instead of the transition between ADP states being rate limiting as it is in MIII, the ATP hydrolysis step is likely rate limiting. In addition, MIII Δ*K* has a higher affinity for actin in both the rigor and ADP states, suggesting the kinase domain may reduce the ability of the motor to bind to actin. Thus, removal of the kinase domain shifts myosin III to a higher duty ratio motor at lower actin concentrations.

One possible explanation for the observed kinetic differences between MIII and MIII Δ*K* is that removal of the kinase domain alters the native structure of myosin IIIA and/or coupling that occurs between the kinase and motor domains. A study that examined the kinetics of *Dictyostelium* myosin II with the N-terminal SH3 domain removed demonstrated reduced ATPase activity, actin binding, and ADP release compared to a wild-type control (*33*). Our results show the complete opposite effect, in that MIII Δ*K* has enhanced ATPase activity, higher actin affinity, and accelerated ADP-release compared to MIII. Therefore, there does not appear to be a conserved role for the N-terminal domain in myosin motor function. Indeed, class I myosins completely lack an N-terminal domain (*2*), suggesting that the importance of the N-terminus varies throughout the myosin superfamily. An intriguing possibility is that kinase-motor interactions influence the kinetic properties of MIII, and that coupling between the motor and kinase domains occurs during the motor ATPase cycle. This may be physiologically relevant because other proteins that interact with myosin IIIA in the cell, such as kinase substrates, may alter the kinase-motor coupling and influence motor activity. Point mutations in the kinase domain will be used in future studies to differentiate between the kinetic effects that are due to alterations in the native structure of myosin IIIA versus coupling that occurs between the kinase and motor domains.

Another possible mechanism for the observed differences between MIII and MIII Δ*K* is that phosphorylation of critical sites on MIII may alter the kinetic properties of the myosin IIIA motor. The steady state measurements in MIII have the caveat that phosphorylation can occur during the timecourse of the experiment (steady-state ATPase and actin binding). However, because the transient kinetic measurements are done on a rapid time scale and autophosphorylation is slow (*3*, *4*), the phosphorylation state will not likely change during the timecourse of these measurements. Western blot analysis demonstrated that the phosphothreonine content in purified MIII and MIII Δ*K* was quite low compared to fully phoshorylated MIII, suggesting phosphorylation itself is not responsible for the transient kinetic differences between the two constructs. However, we cannot rule out that phosphoserine levels are responsible for the kinetic differences, because the phosphoserine content was higher in MIII compared to MIII Δ*K* in the absence of ATP. Further analysis is necessary to confirm the phosphorylation levels of purified MIII and MIII Δ*K* using more sensitive methods such as mass spectrometry. Our results do not rule out that fully phosphorylated MIII may have altered ATPase activity. In order to rigorously examine the effect of phosphorylation on the kinetic properties of MIII, the phosphorylation sites must be determined and point mutations that mimic and prevent phosphorylation examined. Thus, it is possible that future studies will reveal that both kinase-motor interactions and phosphorylation may play a role in regulating the motor

properties of myosin IIIA in sensory cells. In addition, calcium may also play a role in myosin IIIA regulation, but it was not investigated in the current study since all experiments were performed in buffer containing EGTA.

ATP Binding to Myosin III ΔK. We reported that the rate of ATP binding to the myosin IIIA motor domain in the construct containing the kinase domain is quite slow (*4*). We also determined that actin binding enhances the rate of ATP binding to the motor domain of MIII (*4*). Thus, although the kinase domain appears to interfere with ATP binding, this interference is reduced when MIII is bound to actin. Our current results support this conclusion since MIII Δ*K* has a similar ATP binding rate to that of actin bound MIII. In addition, the rate of ATP binding in MIII Δ*K* was similar in the presence and absence of actin. These results suggest coupling between the kinase and motor domain may play a role in the ATP binding step in the absence of actin. Upon binding to actin the kinase-motor interactions that reduce ATP binding may be abolished. Structurally this could be accomplished by altering the position of switch I, a critical element of the nucleotide binding region. Previous results have demonstrated that myosin VI has a reduced ATP binding rate, which is a consequence of interactions between a unique insert and switch I (*33*). The inhibited conformation of switch I may be promoted by specific kinase-motor interactions, while upon binding to actin these interactions are abolished.

The Hydrolysis Step in Myosin III ΔK. The rate of ATP hydrolysis in MIII Δ*K* in the absence of actin may be rate limiting. Both ^{32}P and phosphate release experiments suggest the equilibrium constant for ATP hydrolysis is approximately 1.5 and the rate of ATP hydrolysis is $\sim$3.0 s^{-1}. Kinetic simulations using the measured rate and equilibrium constants demonstrate a turnover rate similar to our measured k_{cat} (data not shown). Actin-activated product release monitored with mantATP suggests that following a delay which allows MIII Δ*K* to populate the M.ADP.Pi state the reaction proceeds at a rate of $\sim$10 s^{-1}. This rate is similar to the fast phase of our ADP release experiments (Figure 7). A similar experiment performed with MIII indicated a slow transition following the hydrolysis step was rate limiting, which we concluded to be the transition between actomyosin.ADP states (*4*).

Our hydrolysis results are similar to the previous report of myosin IIIA without the kinase domain and lacking IQ domains (*16*) in that a similar equilibrium constant for ATP hydrolysis was obtained ($K_3 = 1.5$). In addition, the affinity for actin in the M.ATP state, estimated from light scatter measurements (data not shown), was found to be quite high ($1/K_8 \approx 1$ μM) in our MIII Δ*K* construct. However, the rate of ATP hydrolysis in the absence of actin that we measured was $\sim$10-fold faster and the affinity for actin in the M.ATP state was 10-fold weaker compared to Kambara et al. (*16*). The differences in the kinetic measurements may be due to their removal of the IQ motifs. Indeed, myosin V complexed with different light chains was shown to have different ATP hydrolysis rate and equilibrium constants (*34*). Furthermore, measurements in the Kambara et al. study (*16*) were done at a lower ionic strength than our studies, which is known to alter actin affinity in the weak binding states. Overall, kinetic analysis of the kinase removed myosin IIIA in the current study and the Kambara study (*16*) suggest the predominant steady-state intermediate is the pre-hydrolysis M.ATP state.

We cannot rule out that actin bound hydrolysis occurs in the MIII Δ*K* pathway as was suggested by Kambara et al. (*16*). Because the affinity for actin in the M.ATP state may be quite high, we would expect to observe inhibition of the steady-state ATPase at higher actin concentrations if actin bound hydrolysis did not occur. Since we did not observe this inhibition, our results suggest actin bound hydrolysis may occur in the actoMIII Δ*K* pathway. Nevertheless, the kinetic mechanism of myosin IIIA containing the kinase domain is very different because the actomyosin.ADP state is the predominant steady state intermediate. The steps in the pathway that account for this difference are an equilibrium constant for ATP hydrolysis that is highly favored and a slow transition between actomyosin.ADP states in MIII. Therefore, the kinase domain, either by phosphorylation or kinase-motor coupling, may be important for mediating ATP hydrolysis and ADP release.

Rate-limiting ATP hydrolysis has been reported for very few other myosins. Myosin IXB was found to have rate-limiting ATP hydrolysis and a high affinity for actin in the M.ATP state, which results in the actomyosin.ATP state being the predominant steady-state intermediate (*35*). Myosin IXB was also found to have the ability to move processively along actin (*35*). Myosin II was shown to be limited by actin-bound ATP hydrolysis at low ionic strength and saturating actin concentrations (*27*). However, it is unclear whether this pathway occurs under physiological conditions. Previous work demonstrated that full-length MIII Δ*K* is capable of translocating to the tips of actin bundles in sensory cells and filopodia in COS cells and motor activity is required for myosin IIIA tip localization (*13*, *31*). Thus, it appears that in these cells MIII Δ*K* is capable of functioning as a motor with a rate-limiting hydrolysis step. Therefore, a rate-limiting ATP hydrolysis step appears to be a viable kinetic mechanism for myosin motor function, but it is unclear what advantage this mechanism would provide for myosins to perform their cellular functions.

Scheme 2

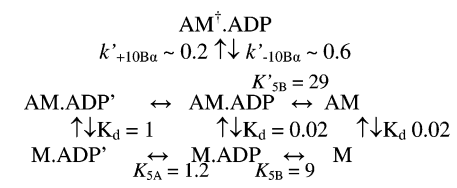

The ADP Release Step in Myosin III ΔK. We found a two-step mantADP release in MIII Δ*K* that was very similar to that of MIII. Similarly, we observed two phases of unlabeled ADP release from pyrene actomyosin III Δ*K* in the presence of 5.0 μM actin. The slow phase of ADP release (0.6−0.7 s^{-1}) was found to be 2-fold slower than the k_{cat} measured in our steady-state ATPase assay. In addition, the slow phase was not observed in the actin-activated product release experiments (Figure 7C). Thus, the slow transition measured by mantADP and pyrene actin may indicate an off-pathway intermediate. A similar off-pathway actomyosin.ADP intermediate was observed in the myosin V ATPase cycle (*36*). Scheme 2 represents a proposed model for the two actomyosin.ADP states and a third off pathway AM†.ADP state.

The proposed AM†.ADP state would have a more quenched pyrene actin fluorescence and more enhanced mantADP fluorescence compared to the AM.ADP′ and AM.ADP states. Evidence for multiple actomyosin.ADP states in MIII Δ*K* is also apparent from the pyrene actin binding experiments in the presence of ADP. We observed fast and intermediate phases with pyrene actin binding that were both linearly dependent on pyrene actin concentrations, and a third phase that was independent of actin concentration. The two actin-dependent phases were modeled to be weak ($1/K_{10A} = 1\ \mu$M) and strong ($1/K_{10B} = 0.02\ \mu$M) actin affinity states. The slow phase of the pyrene actin binding data was modeled to be the transition into the off pathway actomyosin.ADP intermediate ($k'_{+10B\alpha} \approx 0.2\ s^{-1}$). We propose that the transition out of this intermediate is monitored by mantADP release and ADP release from pyrene actomyosin ($k'_{+10B\alpha} \approx 0.6\ s^{-1}$). In our previous study of MIII, we observed a slow transition between the two actomyosin.ADP states that occurred at a similar rate and was similar to the k_{cat}. We concluded that this step is the rate-limiting step in the MIII ATPase cycle. Thus, population of the proposed off-pathway AM.ADP intermediate may be influenced by the kinase domain (i.e., MIII populates the off-pathway AM†.ADP state, whereas MIII Δ*K* does not).

The physiological relevance of multiple actomyosin.ADP states in the myosin ATPase cycle has been proposed in previous studies of other myosins (*36*−*40*). The slow transition between actomyosin.ADP states may allow myosin IIIA to generate tension for a longer period of time under conditions of high mechanical load. In addition, myosin IIIA may be able to function as an efficient transporter under conditions where it proceeds through the rapid ADP-release step, whereas it may function as a tension generator or anchor under conditions where it populates the off-pathway AM†.ADP state.

Model of Myosin IIIA Regulation. Our cell localization studies suggest that full length human myosin IIIA localization to the tips of filopodia is enhanced by removal of the kinase domain. Previous studies have also found that bass myosin IIIA localizes more efficiently to the tips of filopodia in HeLa cells without the kinase domain (*31*). In addition, kinase domain removal results in more enhanced localization of human myosin IIIA to the tips of filopodia in COS cells and inner hair cell stereocilia (*45*) and enlargement of a compartment at the tips (*13*). Our current results add to previous results by demonstrating that HeLa cells transfected with MIII Δ*K* are more likely to contain tip localization than cells transfected with wild type MIII. Because the filopodia in HeLa cells are more pronounced than in COS cells our results demonstrate that MIII is sometimes found localized along the length of the filopodia while MIII Δ*K* is predominantly at the tips. Our results are not able to conclude that more filopodia are present in the MIII Δ*K* tranfected cells compared to MIII transfected cells because numbers of filopodia per cell are highly variable and are present in the non-transfected cells as well. Thus, it remains to be determined if myosin IIIA contains the ability to induce filopodia as has been found with myosin X (*41*).

The enhanced tip localization observed with myosin IIIA Δ*K* may be due to an increase in the rate of movement to the tips. The enhanced ATPase activity and actin binding affinity in MIII Δ*K* suggest that the rate of movement may be increased in MIII Δ*K*, as sliding velocity scales with ATPase rate in many myosins (*42*, *43*). If the kinase domain inactivates or downregulates the motor by phosphorylation or kinase-motor interactions, this may also explain the enhanced tip localization in MIII Δ*K*. The inactivated myosin IIIA could return to the base of actin bundles by retrograde flow. Because myosin IIIA has a tail actin binding motif, it would be able to stay attached to actin when the actin affinity of the motor domain is reduced due to down regulation. Additionally, it is possible that myosin IIIA may have a homologous function to that of myosin IA, which was recently shown to power the motion of the microvillar membrane toward the tips of the microvilli and increase the size of the compartment at the tips (*44*). Indeed, myosin IIIA was shown to contain lipid binding capability in its tail domain (*45*), which would allow the tail to dock onto the membrane while the motor generates tension through its interaction with actin. Further study is necessary to determine the mechanism of myosin IIIA regulation by phosphorylation and/or kinase-motor interactions. Nevertheless, our results suggest the concentration and activity of myosin IIIA localized to the tips of actin bundles may be important for mediating actin bundle tip morphology in sensory cells.

Our results have provided further evidence of kinase-dependent regulation of myosin IIIA both in biochemical and cell biological assays. Our kinetic analysis demonstrates myosin IIIA has a higher actin-affinity and ATPase rate with the kinase domain removed. The hydrolysis step is slow whereas the transition between actomyosin.ADP states is accelerated in the kinase-removed construct, which accounts for the kinetic differences from wild-type myosin IIIA. Thus, the transition between actomyosin.ADP states or hydrolysis could be key regulatory steps in the myosin IIIA motor ATPase cycle.

ACKNOWLEDGMENT

We thank Dr. Howard White for the generous gift of phosphate binding protein. We also thank Dr. Enrique De La Cruz for critically reading and providing comments on the manuscript.

REFERENCES

1. Holmes, K. C., and Geeves, M. A. (1999) Structural mechanism of muscle contraction, *Annu. Rev. Biochem. 68*, 687−728.
2. Sellers, J. R. (1999) *Myosins*, 2nd ed, Oxford University Press, New York, NY.
3. Komaba, S., Inoue, A., Maruta, S., Hosoya, H., and Ikebe, M. (2003) Determination of human myosin III as a motor protein having a protein kinase activity, *J. Biol. Chem. 278*, 21352−21360.
4. Dosé, A. C., Ananthanarayanan, S., Moore, J. E, Burnside, B., and Yengo, C. M. (2007) Kinetic mechanism of human myosin IIIA, *J. Biol. Chem. 282*, 216−231.
5. Montell, C., and Rubin, G. M. (1988) The *Drosophila nina*C locus encodes two photoreceptor cell specific proteins with domains homologous to protein kinases and the myosin heavy chain head, *Cell 52*, 757−772.
6. Porter, J. A., and Montell, C. (1993) Distinct Roles of the *Drosophila nina*C kinase and myosin domains revealed by systematic mutagenesis, *J. Cell Biol. 122*, 601−612.
7. Porter, J. A., Yu, M., Doberstein, S. K., Pollard, T. D., and Montell, C. (1993) Dependence of calmodulin localization in the retina on the NINAC unconventional myosin, *Science 262*, 1038−1042.
8. Dosé, A. C., and Burnside, B. (2000) Cloning and chromosomal localization of human class III myosin, *Genomics 67*, 333−342.

9. Dosé, A. C., and Burnside, B. (2002) A class III myosin expressed in the retina is a potential candidate for bardet-biedl syndrome, *Genomics 79*, 621−624.
10. Dosé, A. C., Hillman, D. W., Wong, C., Sohlberg, L., Lin-Jones, J., and Burnside, B. (2003) Myo3A, one of two class III myosin genes expressed in vertebrate retina, is localized to the calycal processes of rod and cone photoreceptors and is expressed in the sacculus, *Mol. Biol. Cell 14*, 1058−1073.
11. Walsh, T., Walsh, V., Vreugde, S., Hertzano, R., Shahin, H., Haika, S., Lee, M. K., Kanaan, M., King, M., Avraham, K. B. (2002) From flies' eyes to out ears: mutations in a human class III myosin cause progressive nonsyndromic hearing loss DFNB30, *Proc, Natl. Acad. Sci. 99*, 7518−7523.
12. Lin-Jones, J., Parker, E., Wu, M., Dose, A., and Burnside, B. (2004) Myosin 3A transgene expression produces abnormal actin filament bundles in transgenic Xenopus laevis rod photoreceptors, *J. Cell Sci. 117*, 5825−5834.
13. Schneider, M. E., Dosé, A., Salles, F. T., Chang, W., Erickson, F. L., Burnside, B., and Kachar, B. (2006) A new compartment at stereocilia tips defined by special and temporal patterns of myosin IIIa expression, *J. Neurosci. 26*, 10243−10252.
14. Cronin, M. A., Diao, F., and Tsunada, S. (2004) Light-dependent subcellular translocation of Gqalpha in Drosophila photoreceptors is facilitated by photoreceptor specific myosin III NINAC, *J. Cell Sci. 117*, 4797−4806.
15. Lee, S. J., and Montell, C. (2004) Light-dependent translocation of visual arrestin regulated by the NINAC myosin III, *Neuron 43*, 95−103.
16. Komaba, T., Komaba, S., and Ikebe, M. (2006) Human myosin III is a motor having an extremely high affinity for actin, *J. Biol. Chem. 281*, 37291−37301.
17. Hiratsuka, T. (1983) New ribose-modified fluorescent analogs of adenine and guanine nucleotides available as substrates for various enzymes, *Biochim. Biophys. Acta 742*, 496−508.
18. Woodward, S. K., Eccleston, J. F., and Geeves, M. A. (1991) Kinetics of the interaction of 2′(3′)-O-(N-methylanthraniloyl)-ATP with myosin subfragment 1 and actomyosin subfragment 1: characterization of two acto-S1-ADP complexes, *Biochemistry 30*, 422−430.
19. Sweeney H. L., Rosenfeld S. S., Brown F., Faust L., Smith J., Xing J., Stein L. A., Sellers J. R. (1998) Kinetic tuning of myosin via a flexible loop adjacent to the nucleotide binding pocket, *J. Biol. Chem. 273*, 6262−6270.
20. Sun, M., Oakes, J. L., Ananthanarayanan, S. K., Hawley, K. H., Tsien, R. Y., Adams, S. R., and Yengo, C. M. (2006) Dynamics of the upper 50 kDa domain of myosin V examined with fluorescence resonance energy transfer, *J. Biol. Chem. 281*, 5711−5717.
21. Pardee, J. D., and Spudich, J. A. (1982) Purification of muscle actin, *Methods Enzymol. 85*, 164−181.
22. Pollard, T. D. (1984) Polymerization of ADP-actin, *J. Cell Biol. 99*, 769−777.
23. De La Cruz, E. M., Sweeney, H. L, and Ostap, E. M. (2000) ADP inhibition of myosin V ATPase activity, *Biophys. J. 79*, 1524−1529.
24. White, H. D., and Rayment, I. (1993) Kinetic characterization of reductively methylated myosin subfragment 1, *Biochemistry 32*, 9859−9865.
25. Yengo, C. M., De La Cruz, E. M., Safer, D., Ostap, E. M., and Sweeney, H. L. Kinetic characterization of the weak binding states of myosin V. (2002), *Biochemistry 41*, 8508−8517.
26. Brune, M., Hunter, J. L., Corrie, J. E., and Webb, M. R. (1994) Direct, real-time measurement of rapid inorganic phosphate release using a novel fluorescent probe and its application to actomyosin subfragment 1 ATPase, *Biochemistry 33*, 8262−8271.
27. White, H. D., Belknap, B., and Webb, M. R. (1997) Kinetics of nucleoside triphosphate cleavage and phosphate release steps by associated rabbit skeletal actomyosin, measured using a novel fluorescent probe for phosphate, *Biochemistry 36*, 11828−11836.
28. Henn, A., and De La Cruz, E. M. (2005) Vertebrate myosin VIIb is a high duty ratio motor adapted for generating and maintaining tension, *J. Biol. Chem. 280*, 39665−39676.
29. Robblee, J. P., Olivares, A. O., and De La Cruz, E. M. (2004) Mechanism of nucleotide binding to actomyosin VI: evidence for allosteric head-head communication, *J. Biol. Chem. 37*, 38608−38617.
30. De La Cruz, E. M., Ostap, E. M., and Sweeney, H. L. (2001) Kinetic mechanism and regulation of myosin VI, *J. Biol. Chem. 274*, 32373−32381.
31. Erickson, F. L., Corsa, A. C., Dosé, A. C., and Burnside, B. (2003) Localization of a class III myosin to filopodia tips in transfected HeLa cells requires an actin-binding site in its tail domain, *Mol. Biol. Cell 14*, 4173−4180.
32. Fujita-Becker, A., Tsiavaliaris, G., Ohkura, R., Shimada, T., Manstein, D. J., and Sutoh, K. (2006) Functional characterization of the N-terminal region of myosin-2, *J. Biol. Chem. 281*, 36102−36109.
33. Menetrey, J., Bahloul, A., Wells, A. L., Yengo, C. M., Morris, C. A., Sweeney, H. L., and Houdusse, A. (2005) The structure of the myosin VI motor reveals the mechanism of directionality reversal, *Nature 435*, 779−785.
34. De La Cruz, E. M., Wells, A. L., Sweeney, H. L., and Ostap, E. M. (2000) Actin and light chain isoform dependence of myosin V kinetics, *Biochemistry 39*, 14196−14202.
35. Kambara, T., and Ikebe, M. (2006) A unique ATP hydrolysis mechanism of single-headed processive myosin, myosin IX, *J. Biol. Chem. 281*, 4949−4957.
36. Hannemann, D. E., Cao, W., Olivares, A. O., Robblee, J. P., and De La Cruz, E. M. (2005) Magnesium, ADP, and actin binding linkage of myosin V: evidence for multiple myosin V-ADP and actomyosin V-ADP states, *Biochemistry 44*, 8826−8840.
37. Uemura, S., Higuchi, H., Olivares, A. O., De La Cruz, E. M., and Ishiwata, S. (2004) Mechanochemical coupling of two substeps in a single myosin V motor, *Nat. Struct. Mol. Biol. 11*, 877−883.
38. Mehta, A. D., Rock, R. S., Rief, M., Spudich, J. A., Mooseker, M. S, and Cheney, R. E. (1999) Mechanochemical coupling of two substeps in a single myosin V motor, *Nature 400*, 590−593.
39. Nyitrai, M., and Geeves, M. A. (2004) Adenosine diphosphate and strain sensitivity in myosin motors, *Philos. Trans. R. Soc. Lodon Ser. B 359*, 1867−1877.
40. Conibear, P. B. (1999) Kinetic studies on the effects of ADP and ionic strength on the interaction between myosin subfragment-1 and actin: implications for load-sensitivity and regulation of the crossbridge cycle, *J. Muscle Res. Cell Motil. 20*, 727−742.
41. Bohil, A. B., Robertson, B. W., and Cheney, R. E. Myosin-X is a molecular motor that functions in filopodia formation, *Proc. Natl. Acad. Sci. U.S.A. 103*, 12411−12416.
42. Barany, M. (1967) ATPase activity of myosin correlated with speed of muscle shortening, *J. Gen. Physiol. 50*(Suppl), 218.
43. Tyska, M. J., and Warshaw, D. M. (2002). The myosin power stroke, *Cell Motil. Cytoskeleton 51*, 1−15.
44. McConnell, R. E., Tyska, M. J. (2007). Myosin-1a powers the sliding of apical membrane along microvillar actin bundles, *J. Cell Biol. 177*, 671−681.
45. Dosé, A. C., Yengo, C. M., and Burnside, B. (2007). Binding substrates of the photoreceptor-expressed human class III myosin, MYO3A. *FASEB Summer Research Conferences: Biology and Chemistry of Vision*, June 16−21, 2007.

BI7021574